HEALTH AND MEDICINE

# Electrophoretic drug delivery for seizure control

**Christopher M. Proctor[1,2]*, Andrea Slézia[3]*, Attila Kaszas[3†], Antoine Ghestem[3], Isabel del Agua[2], Anna-Maria Pappa[1,4], Christophe Bernard[3], Adam Williamson[3‡], George G. Malliaras[1,2‡]**



**The persistence of intractable neurological disorders necessitates novel therapeutic solutions. We demonstrate the utility of direct in situ electrophoretic drug delivery to treat neurological disorders. We present a neural probe incorporating a microfluidic ion pump (μFIP) for on-demand drug delivery and electrodes for recording local neural activity. The μFIP works by electrophoretically pumping ions across an ion exchange membrane and thereby delivers only the drug of interest and not the solvent. This "dry" delivery enables precise drug release into the brain region with negligible local pressure increase. The therapeutic potential of the μFIP probe is tested in a rodent model of epilepsy. The μFIP probe can detect pathological activity and then intervene to stop seizures by delivering inhibitory neurotransmitters directly to the seizure source. We anticipate that further tailored engineering of the μFIP platform will enable additional applications in neural interfacing and the treatment of neurological disorders.**

## INTRODUCTION

The failure of systemic drug treatments to address numerous neurological disorders has spurred the development of alternative approaches that attempt localized treatment. These localized treatments focus therapy on the region of the brain affected by the pathology, thereby enhancing the effectives of the treatment while reducing side effects inherent in systemic treatments. Some of these approaches such as optogenetics (*1*–*4*) and designer receptors exclusively activated by designer drugs (*5*) have shown promise but have been limited by safety concerns about the need for viral transfer of engineered proteins and molecules (*6*). Other treatments such as syringe injection or convection-enhanced delivery of drugs are prone to clogging or reflux and may also cause local edemas due to the pressure increase at the injection point (*7*–*9*).

In this work, we show that electrophoretic drug delivery can overcome the above problems by coupling the benefits of a highly localized, on-demand treatment with drugs that specifically control cellular functions. We demonstrate the therapeutic potential using epilepsy as a model system. Epilepsy, which affects 1% of the world population and remains drug-resistant in 30% of the cases (*10*, *11*), is a prototypical example for which systemic drugs have failed in the clinic despite having strong antiepileptic effects because of their side effects, toxicity, and/or failure to cross the blood-brain barrier (*12*). The intermittent nature of epileptic seizures makes the disorder particularly well suited for a therapeutic approach such as electrophoretic drug delivery that acts only when needed, for instance, just before the onset of a seizure.

Here, we present an electrophoretic drug delivery device based on the organic electronic ion pump (OEIP), which offers the ability to deliver drugs with precise spatiotemporal control (*13*, *14*). In contrast to other drug delivery devices, the ion pump works by electrophoretically pumping ions across an ion exchange membrane and thereby delivers only the drug of interest and not the solvent (aside from a few water molecules per ion that make up the hydration shell). This "dry" delivery is of paramount importance for biological interfacing as it enables an intimate interface between the drug delivery outlet and the target cells, allowing large amounts of drug delivery with negligible local pressure increase. Previous reports of OEIPs have shown much promise for interfacing with biology; however, challenges in scaling down these devices have limited their in vivo applications within the brain to date (*15*–*19*).

To that end, we engineered neural probes incorporating an ion pump for on-demand drug delivery and electrodes for recording local neural activity (Fig. 1A). The implant features a modified version of the OEIP known as a microfluidic ion pump (μFIP), which significantly reduces the voltage required to deliver ions (drugs) and simplifies replenishing/exchanging the ion reservoir (*20*). The μFIP implant features a U-shaped microfluidic channel (cross-section, 50 μm × 40 μm) formed using photocurable epoxy (SU8) layers for the base and walls (10 and 40 μm in thickness, respectively) and a parylene-C top layer (4 μm in thickness). Fabrication of the SU-8/parylene–based microfluidic channel was enabled by a novel solid-on-liquid fabrication approach (*21*) using capillary patterning, as shown in fig. S1 and described in Materials and Methods. Small holes (15 μm diameter) etched through the parylene-C layer at the end of the implant coated with a poly(styrenesulfonate) (PSS)–based anion exchange membrane (6 μm in thickness) serve as the drug delivery outlet for μFIP, while a gold electrode (150 nm) at the base of the fluidic channel serves as the ion pump source electrode. The ion pump outlets are flanked by two poly(3,4-ethylenedioxythiophene):PSS (PEDOT:PSS)–coated (2 μm thickness) electrodes for recording local electrophysiological activity with superior signal-to-noise ratio (*22*).

## RESULTS

The drug delivery capability of the probe was tested in a bath of artificial cerebrospinal fluid (ACSF) by loading the microfluidic channel with an aqueous solution of the drug of interest and applying up to 1 V between the source electrode and an external target

[1]Electrical Engineering Division, University of Cambridge, Cambridge CB3 0FA, UK. [2]Department of Bioelectronics, Ecole Nationale Supérieure des Mines, CMP-EMSE, 13541 Gardanne, France. [3]Aix Marseille Université, Institut de Neurosciences des Systèmes, UMR_S 1106, 13005 Marseille, France. [4]Department of Chemical Engineering and Biotechnology, University of Cambridge, Cambridge CB2 3RA, UK.
*These authors contributed equally to this work.
†Present address: Aix-Marseille Université, Institut de Neurosciences de la Timone, CNRS UMR 7289, 13005 Marseille, France.
‡Corresponding author. Email: gm603@cam.ac.uk (G.G.M.); adam.williamson@univ-amu.fr (A.W.)

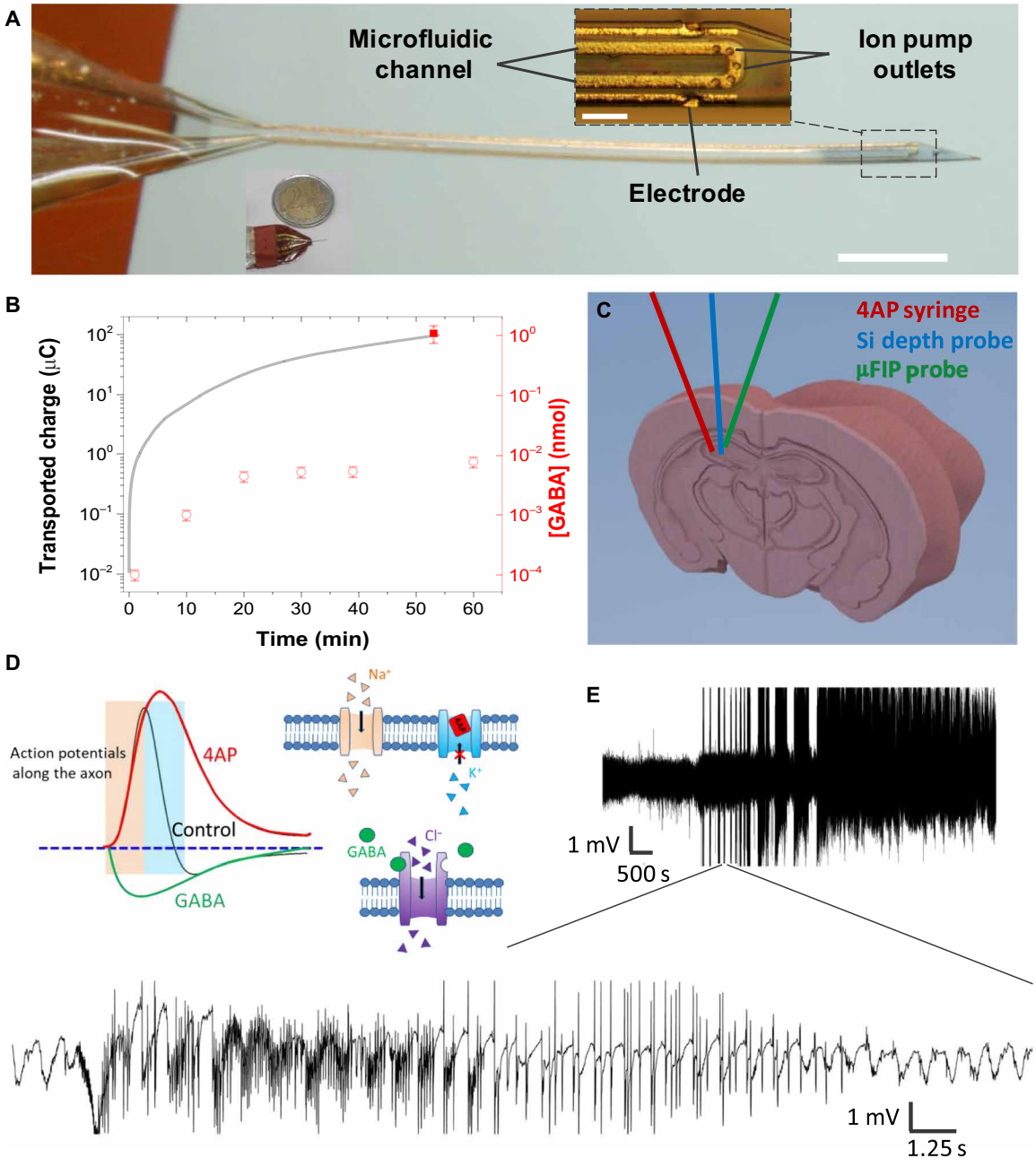


**Fig. 1. Overview of the μFIP probe.** (**A**) Implanted end of the device (inset scale bar, 100 μm; outside scale bar, 1 mm). (**B**) Net transported charge across the ion bridge when actively pumping GABA at 1 V (line, left axis), [GABA] passively diffused out of the device when no voltage was applied (open symbols, right axis), and [GABA] actively pumped out of the device at 1 V (closed symbols, right axis). (**C**) Schematic showing placement of syringe for 4AP injection, Si depth probe, and the μFIP probe in the hippocampus. (**D**) Conceptual illustration showing a proposed effect of 4AP on $K^+$ channels and action potentials (*31*) along with the analogous effects of GABA. (**E**) Representative recording of intense SLEs following injection of 4AP at two different time scales.

electrode. We found that the μFIP probe is capable of pumping a variety of small positively charged ions with important biological functions including $K^+$, $Ca^{2+}$, acetylcholine, and γ-aminobutyric acid (GABA). Taking GABA delivery as an example, the net transported charge across the device operated at 1 V as a function of time is shown in Fig. 1B (solid line, left *y* axis) along with the net amount of GABA delivered from the device (closed symbol, right axis). The close agreement between the net transported charge and the amount of GABA delivered indicates that the μFIP operates with a pumping efficiency approaching unity, meaning nearly all the ions transported across the anion exchange membrane are the drug of interest. Figure 1B shows that the probe can deliver in excess of $10^{-3}$ nmol of GABA within seconds. Taking a volume defined by the diffusion length of a cationic neurotransmitter (*23*, *24*), the μFIP can thus quickly tune the local concentration of GABA above $10^{-5}$ M, which is within the range demonstrated to inhibit neural activity (*25*, *26*).

The passive diffusion of GABA out of the μFIP in the absence of an applied bias was roughly two orders of magnitude less than the active pumping rate (Fig. 1B, open symbols, right *y* axis). This suggests that, even ignoring the existing powerful GABA uptake mechanisms, passive diffusion alone cannot raise extracellular GABA concentrations enough to inhibit local activity (*20*).

Having benchmarked the drug delivery capacity, we used epilepsy as a model system to test the therapeutic potential of the μFIP implant. Seizure-like events (SLEs) were induced by local injection of 4-aminopyridine (4AP) into the hippocampus of anesthetized mice following previously reported procedures (Fig. 1C) (*27*–*30*). 4AP has been suggested to block certain voltage-gated $K^+$ channels, which increases the necessary repolarization time for neurons, essentially leaving the intracellular potential positive for longer periods of time, leading to the synchronous firing of larger populations of neurons (Fig. 1D) and ultimately SLEs (*31*). We chose to use GABA as a therapeutic agent because it is an endogenous inhibitory compound that can be quickly metabolized after delivery, thus limiting the potential deleterious effects of long-term network activity shutdown. GABA inhibits neural activity by inducing uptake of $Cl^-$ (Fig. 1D), thereby lowering the intracellular potential and correspondingly the ability of a neuron to fire. Previous in vitro work indicated that GABA can be effective for stopping 4AP-induced epileptiform activity (*16*, *18*). The inducible SLE model was developed by testing a range of 4AP concentrations with and without concurrent implantation of the μFIP probe loaded with GABA at the 4AP injection site (see Materials and Methods). Figure 1E shows a representative recording of neural activity in the hippocampus from one of the channels of a 32-channel silicon depth probe implanted in the space immediately adjacent to the 4AP injection site (Fig. 1C). The recording sites of the Si probe were spaced in a linear array with 100 μm between recording sites, allowing simultaneous recording in the cortex as well as the hippocampus. Interictal spikes observable on all recording channels of the Si probe were observed within 20 min of injection, indicating that the local 4AP injection led to coordinated pathological events far beyond the injection site. The onset of interictal spikes was typically followed by increasingly intense SLEs lasting several seconds and, with larger doses, the onset of status epilepticus (uninterrupted SLE lasting more than 1 hour). The response to 4AP injection was the same regardless of the presence of the unactivated μFIP implant, indicating that neither the physical presence of the implant nor the passive diffusion of GABA from the probe had a significant effect on SLE induction.

After validating the SLE model, we tested the therapeutic capability of electrophoretic drug delivery by using the μFIP probe to deliver GABA at the 4AP injection site. Electrophysiology recordings from the ion pump electrodes were observed following the 4AP injection, and the ion pump was turned on immediately following the first pathological events. Representative recordings from the injection site show the stark contrast between the case of no μFIP treatment (Fig. 2A) compared to μFIP treatment initiated immediately after the first SLE (Fig. 2B). In the case of the μFIP intervention, no additional SLEs were observed after initiating the GABA delivery (Fig. 2B, green arrow), whereas mice with 4AP dosing and no μFIP intervention developed additional seizures lasting over an hour.

As promising as these results are, a treatment that could prevent all pathological events would be preferable to a treatment that is only

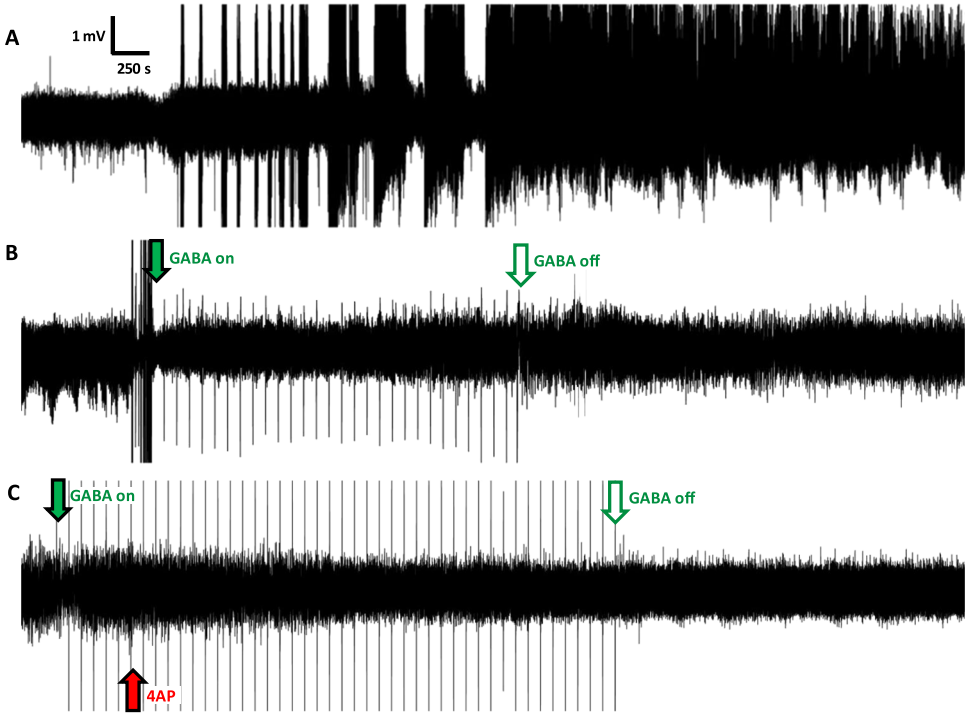


**Fig. 2. Representative electrophysiology recordings from the hippocampus.** (**A**) Recording in the absence of the μFIP treatment with SLEs starting approximately 30 min after 4AP injection followed by status epilepticus. (**B**) Recording of case in which the μFIP treatment was initiated immediately following the first SLE, showing no further pathological events after the treatment starts. (**C**) Recording in which the μFIP treatment was initiated before 4AP injection, showing no pathological events. Red arrow indicates 4AP injection. Solid green arrows indicate start of the μFIP treatment, and open green arrows mark the end of the μFIP treatment. Sharp peaks at 100-s intervals following green arrow are artifacts from the μFIP treatment.

enacted after a pathological and potentially damaging activity has already started. With that in mind, the ability to prevent pathological activity was subsequently tested by initiating the μFIP treatment (Fig. 2C, green arrow) before the 4AP injection (Fig. 2C, red arrow). Neither interictal spikes nor seizures were observed when the GABA delivery was initiated before the 4AP injection. Figure 3 overviews the frequency of pathological events for the control experiments with 4AP injection but no GABA delivery ($n$ = 8), the case of GABA delivery after 4AP injection ($n$ = 3), and the case of GABA delivery before 4AP injection ($n$ = 4) (see table S1 for the complete data set). The decrease in pathological activity was found to be significant ($P < 0.05$) in the case of delivering GABA before 4AP relative to the control experiments. This finding opens the door to coupling electrophoretic drug delivery with advanced electrophysiology analysis algorithms that have shown promise for predicting the onset of seizures (*32*–*35*), thereby enabling a closed loop system that could prevent pathological events before they occur.

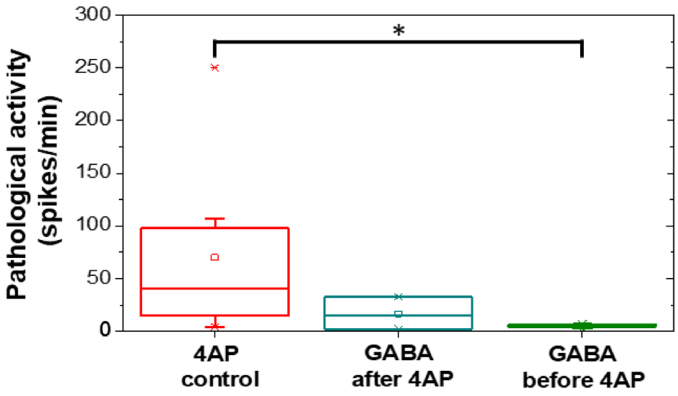


**Fig. 3. Frequency of pathological activity recorded for control experiments with only 4AP as well as for the case of delivering GABA after 4AP and the case of GABA before 4AP.**

Control experiments delivering an equivalent dose of $Na^+$ in place of GABA did not have a notable effect on 4AP-induced activity (table S1), demonstrating that it is not the applied current from the ion pump that modulates electrophysiological activity but rather the delivered molecules. This illustrates the importance of choosing the appropriate drug of interest and effectively rules out the small current stimulus (average, <35 nA) associated with the μFIP operation as the primary therapeutic mechanism.

The lasting effect of the μFIP treatment was explored by administering a second injection of 4AP several minutes after completion of an initial period of GABA delivery. As shown in Fig. 4, in the

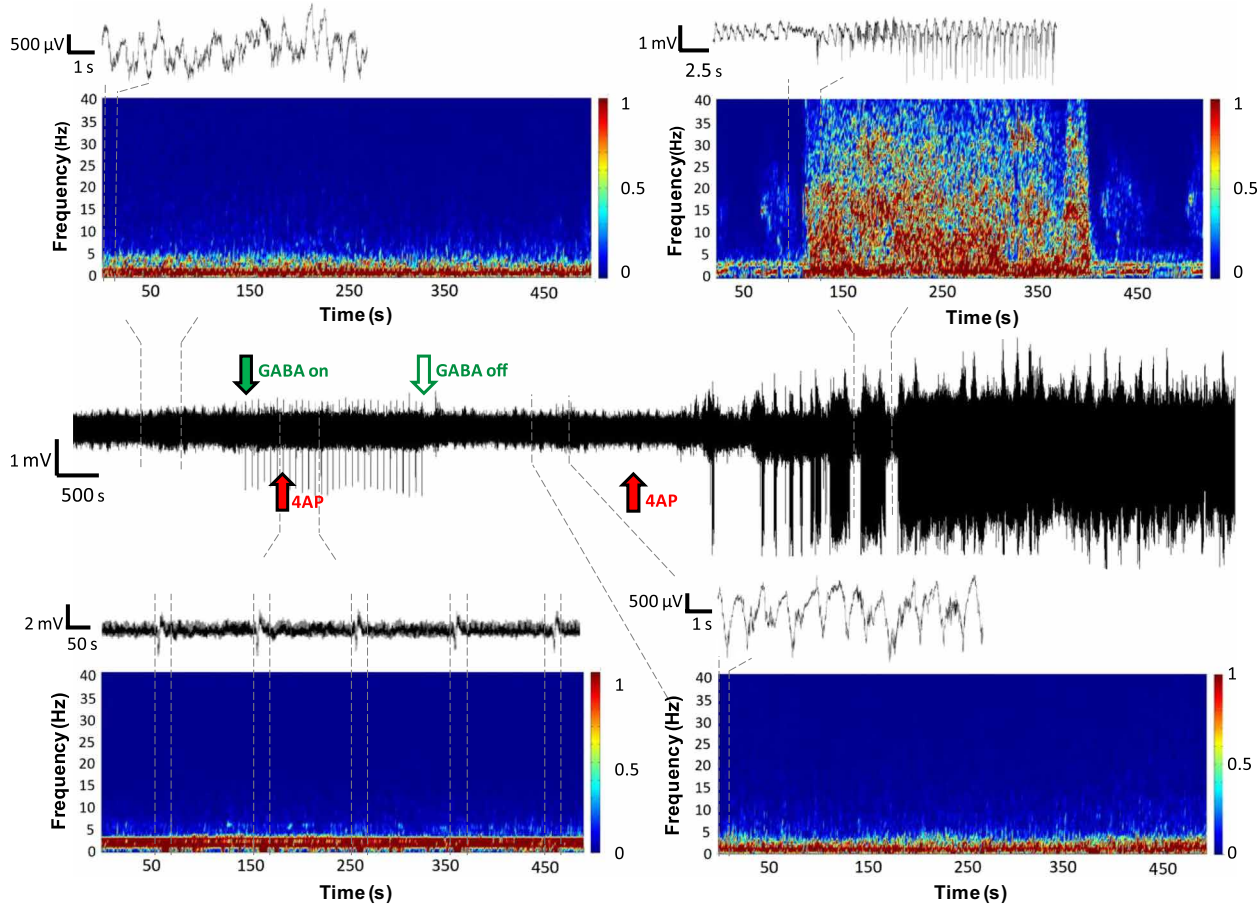


**Fig. 4. Representative recording from an anesthetized mouse given a 4AP injection during a period of GABA delivery (solid green arrow until open green arrow) followed by a second 4AP dose administered several minutes after the μFIP treatment was stopped.** Time/frequency plots for periods before (top left), during (bottom left), and after GABA delivery (bottom right) as well as during an SLE event (top right) are shown along with recording windows for shorter time scales. Dashed lines indicate the time periods covered by each time/frequency and recording plot.

absence of additional GABA delivery, the second 4AP injection induced a series of intense SLEs. This suggests that, as expected, the initial dose of GABA was rapidly metabolized, which is important for avoiding potential side effects that may otherwise occur from maintaining elevated levels of GABA.

The effect of the μFIP treatment was further explored by analyzing the recordings in frequency domain. Figure 4 highlights time/frequency plots for periods before, during, and after the μFIP treatment as well as during SLEs induced by a second dose of 4AP. Low-frequency activity (1 to 5 Hz) characteristic of physiological activity in anesthetized mice was observed in the periods before, during, and after the μFIP operation, while the SLE period featured frequencies up to 40 Hz. Recording artifacts from the μFIP operation featured as periodic low-frequency activity (<1 Hz) in the time/frequency plot during the μFIP treatment. The persistence of physiological rhythms despite GABA delivery suggests that while the GABA dosing was sufficient to stop pathological events, it had only negligible effects on physiological activity. We presume that this is due to the highly localized dosing of relatively small amounts of GABA (less than 1.5 nmol over 50 min).

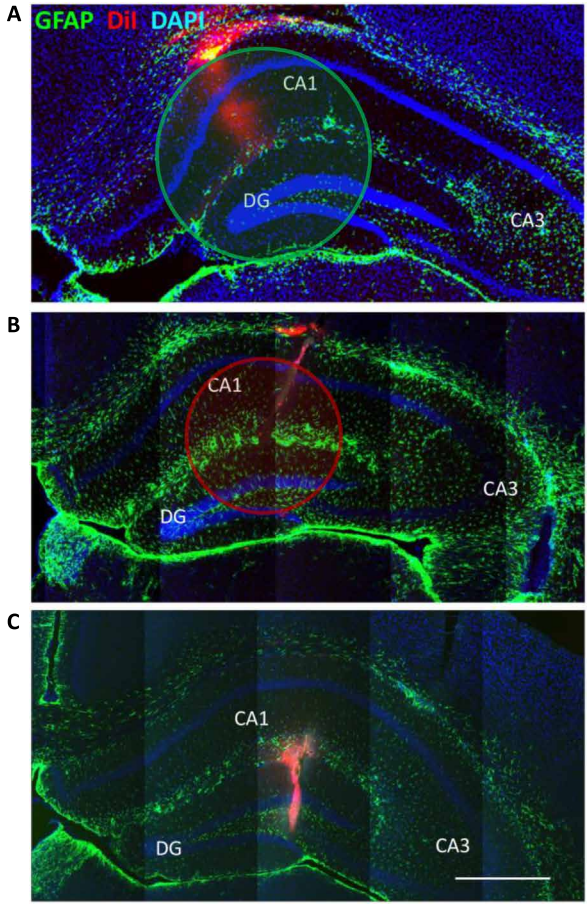


**Fig. 5. Representative histological evaluation of implant traces.** (**A**) μFIP implant, (**B**) 4AP syringe, and (**C**) multichannel Si electrode in the hippocampus. The implants were labeled with DiI and shown as red traces. Astrocytes were labeled in green [glial fibrillary acidic protein (GFAP)], while all cellular nuclei were stained in blue [4′,6-diamidino-2-phenylindole (DAPI)]. Major regions of the hippocampus were labeled in white [cornu ammonis 1 (CA1), cornu ammonis 3 (CA3), and dentate gyrus (DG)]. Scale bar, 500 μm.

As a final analysis, we verified the localization of the three implants by histology and estimated the area of influence of the μFIP probe. Representative traces of the μFIP probe, 4AP injection syringe, and Si depth probe can be seen in the histology slices in Fig. 5 (A, B, and C, respectively). The implants were labeled with 1,1′-dioctadecyl-3,3,3′,3′-tetramethylindocarbocyanine perchlorate (DiI; shown in red) to visualize the trace (see Materials and Methods). The histology confirms placement in the hippocampus, with the outlets of the μFIP probe placed within approximately 300 μm of the tip of the 4AP syringe. The area of influence of the μFIP probe was estimated by a half sphere centered on the outlets of the ion pump with a radius of approximately 550 μm equal to the average diffusion length of a cationic neurotransmitter in extracellular space after 1000 s (Fig. 5A, green circle) (*23*, *24*). This estimated area extends across the hippocampus and encompasses the volume of the injected 4AP solution (Fig. 5B, red circle). We note, however, that this may underestimate the effect of inherent uptake mechanisms for GABA, which might decrease the diffusion length (*23*, *36*, *37*). Likewise, it should be expected that the area of influence would vary depending on the drug of interest, with smaller molecules not native to the body likely diffusing further (*23*).

## DISCUSSION

Having demonstrated here the utility of μFIP treatment in an acute study, we note that further technological developments will be required to enable chronic testing. To that end, the μFIP platform can readily adapt lessons learned from the development of other medical implants with regard to engineering long-term biostability (*38*, *39*), reducing foreign body response (*40*, *41*), and incorporating closed-loop actuation (*42*–*44*). In terms of drug reservoir capacity, it is of note that the μFIP implants in this study were not connected to a fluidic pump during treatment and the small amount of delivered drug found to be effective represents less than 1% of the total drug capacity loaded in the implants. This suggests that chronic μFIP treatment may only require relatively infrequent reloading of the drug reservoir.

Looking ahead, we believe that electrophoretic drug delivery devices can be further adapted to best treat epilepsy and other neurological disorders. While epilepsy is particularly challenging as it presents in many forms, it has been found that approximately 60% of the patients have a single focal point (*45*), and these are the patients that are most likely to find conventional drug treatments inadequate (*46*). Thus, a single μFIP implant at the seizure focus may prove a viable treatment option for these patients. On the other hand, patients with nonfocal epilepsy may benefit from the use of multiple μFIP implants and/or a single implant with multiple drug delivery outlet locations. In addition to epilepsy, we foresee that a μFIP implant could be used, for instance, to deliver dopamine for the treatment of Parkinson's disease with the possibility of using integrated recording sites to optimize the dosing frequency. Likewise, a μFIP implant could deliver chemotherapeutic agents to an inoperable brain tumor and/or to the tissue surrounding a resected tumor. These topics will be the subject of future research.

Here, we have introduced a neural probe incorporating electrophoretic drug delivery and recording capabilities. The drug delivery is made possible by an integrated μFIP, which can deliver small ions such as neurotransmitters on demand via electrophoresis through an ion

exchange membrane. The μFIP probe demonstrated the capability to detect, stop, and even completely prevent SLEs in an animal model by timely delivery of inhibitory neurotransmitters to the seizure source. Although this work is focused on epilepsy treatment, we anticipate that tailored engineering of the μFIP platform will enable additional applications for electrophoretic drug delivery in neural interfacing and the treatment of neurological disorders.

## MATERIALS AND METHODS

### μFIP probe fabrication

Probes were fabricated following standard photolithography practices using plastic photomasks (Selba), a SUSS MJB4 contact aligner, and an SCS Labcoater 2. Glass sides with dimensions of 50 × 76 mm were cleaned and coated with 2-μm-thick parylene-C. The base layer was subsequently formed by selective ultraviolet (UV) exposure (201 mJ/cm$^2$) and development of a 10-μm-thick spin-coated SU8 film (SU-8 2000 series, MicroChem). A photoresist liftoff process using Oscar 5001 (Orthogonal) was used to pattern gold interconnects (2-nm Cr, 150-nm Au) deposited by thermal evaporation. Following Au liftoff, substrates were activated with 100-W $O_2$ plasma (Oxford RIE 80 plus) for 1 min and spin-coated with a 40-μm-thick SU8 layer. Selective UV exposure and development of the SU8 layer formed the walls of the microfluidic channel. Substrates were rinsed with acetone and deionized (DI) water and then activated for 15 s with a 30-W $O_2$ plasma before filling the fluidic channel with 2 μl of 1-butyl-3-methylimidazolium chloride (Alfa Aesar) dissolved in DI water (680 mg/ml). Approximately 4 μm of parylene-C was deposited on the substrates, thereby encapsulating the ionic liquid within the fluidic channel. AZ9260 was subsequently spin-coated, exposed, and developed using MF-26A, followed by reactive ion etching to open the probe outline, electrode openings, fluidic connections ports, and ion pump outlets. Residual photoresist was rinsed away with acetone and isopropyl alcohol, and then rubber adhesive fluidic connectors were applied to the fluidic inlet/outlets before removing probes from the parylene-coated glass substrates using a razor blade. The upper part of the free-standing probes was glued to Kapton substrates (500HN, 127 μm thick) for added structural support (not including the implantable shank). Following 1 min of 100-W $O_2$ plasma activation, the first 0.5 mm of the probe tips was dip-coated into an aqueous dispersion of PEDOT:PSS (PH 1000 from H.C. Stark) containing 5 volume percent (volume %) of ethylene glycol, 0.1 volume % of dodecyl benzene sulfonic acid, and 1 weight % of 3-glycidoxypropyltrimethoxysilane. The devices were then placed in an oven at 120°C for 1 hour. After cooling to room temperature, the microfluidic channels were flushed with DI water at a rate of 5 μl/min for 30 min. The PEDOT:PSS covering the ion pump outlets was then selectively exposed to a 10% solution of sodium hypochlorite (Sigma-Aldrich) by flushing the fluidic channel with the solution at a rate of 2 μl/min for 30 s, followed by 45 min of flowing DI water.

### μFIP probe characterization

μFIP probes were characterized by loading the microfluidic channel with an aqueous solution containing the drug of interest (for example, 0.05 M GABA in DI water) and then placing the probe shanks into a solution of ACSF containing a PEDOT:PSS-coated head screw equivalent to that used for in vivo measurements. A Keithley 2612A Source Measure unit with customized LabVIEW software was used to apply a voltage between the source electrode and the target head screw and measure the resulting current.

### Quantification of GABA in the target electrolyte

The microfluidic channel was filled with a GABA source solution (0.05 M in DI water), and the probe shank was placed into 500 μl of ACSF solution with a PEDOT:PSS-coated headscrew. One-volt pulses were applied between the source and target electrodes (100 s on, 1 s off), while the current was measured. The target solution was then collected, and the concentration of GABA was measured using a GABA enzyme-linked immunosorbent assay (ELISA) kit (ImmuSmol) according to the manufacturer's instructions. For the diffusion measurements, we first ensured that the ion bridge was already filled with ions by running the devices at 1 V for 100 s. We then changed the target solution and started the diffusion measurements. Diffusion time points less than 20 min were estimated on the basis of a linear extrapolation to time zero. Both active pumping and diffusion data points represent the average of at least three samples.

### 4AP seizure model

The voltage-gated $K^+$ channel blocker was injected locally with a programmable automatic pump into the pyramidal layer of CA1 hippocampus to induce local epileptic seizure. One injection of 250 nl of 25 or 50 mM 4AP dissolved in ACSF was injected to the left hemisphere of the mouse hippocampus. Neuronal activity was recorded 1 hour before 4AP injection for control. In every experiment, neuronal activity was recorded for a minimum of 2 hours following drug administration.

### Surgery and recording

Seventeen adult male *OF1* mice were used for the experiments. Mice were entrained to a 12-hour/12-hour light/dark cycle with food and water available ad libitum. All experimental procedures were performed according to the ethical guidelines of the Institut de Neuroscience des Systèmes and approved by the local Ethical Committees and Veterinary Offices. Surgeries and experiments were done under ketamine/xylazine anesthesia (ketamine, 100 mg/kg; xylazine, 10 mg/kg body weight). Mice were fixed in a mouse stereotaxic frame (Kopf Instruments). After a subcutaneous injection of the local painkiller ropivacaine, craniotomy was made from bregma (anteroposterior, 1.0 mm; mediolateral, 1.2 mm; dorsoventral, 2.8 mm from the surface). Skull was opened; dura was removed; and silicon probe (NeuroNexus), μFIP probe, and a Hamilton syringe for 4AP injection with a borosilicate glass capillary (inside diameter, 0.86 mm; outside diameter, 1.5 mm) were lowered into the hippocampus. Capillary was pulled with a pipette puller (P-1000, Sutter Instrument). The tip of the capillary was between 50 and 100 μm. Recordings were made with a 64-channel Neuralynx amplifier.

### Electrophysiology recording analysis

For pathological spike detection, the hippocampal local field potential from the CA1 pyramidal layer was down-sampled and band pass–filtered. CA1 pyramidal layer was chosen on the basis of trace localization in histology images. Spike events were identified when the envelope was at least 3 SDs above the baseline by a semiautomatic method, identifying interictal spikes and epileptic spike activity (*47*). The frequency of the pathological spike activity was calculated 2 hours following drug administration.

### Histology and immunocytochemistry

Animals were transcardially perfused first with saline and then with 150 ml of fixative solution containing 4% paraformaldehyde in 0.1 M phosphate buffer (PB). Tissue blocks were cut on a vibratome (Leica VT1200S, Leica Microsystems) into 40-µm coronal sections. After extensive washes in PB, GFAP staining was used [GFAP Monoclonal Antibody (GA5), Alexa Fluor 488, Thermo Fisher]. Electrodes, syringes, and ion pumps (occasionally) were covered by DiI (NeuroTrace DiI, Thermo Fisher) for the visualization of the traces. Sections were mounted on SuperFrost slides and covered with a mounting medium containing DAPI (VECTASHIELD Antifade Mounting Medium with DAPI, Vector Laboratories). Confocal images were acquired with a Zeiss LSM 510 confocal microscope using either a 10× or a 20× objective with the *z*-stack tiling function of the acquisition software (ZEN).

## SUPPLEMENTARY MATERIALS

Supplementary material for this article is available at http://advances.sciencemag.org/cgi/content/full/4/8/eaau1291/DC1

Fig. S1. Overview of basic fabrication steps and materials used to make µFIP probes.

Fig. S2. Low-magnification image of the coronal sections of the brain containing the three devices.

Table S1. Frequency of pathological activity from in vivo experiments.

## REFERENCES AND NOTES


1. J. T. Paz, J. T. Paz, T. J. Davidson, E. S. Frechette, B. Delord, I. Parada, K. Peng, K. Deisseroth, J. R. Huguenard, Closed-loop optogenetic control of thalamus as a tool for interrupting seizures after cortical injury. *Nat. Neurosci.* **16**, 64–70 (2013).
2. C. Armstrong, E. Krook-Magnuson, M. Oijala, I. Soltesz, Closed-loop optogenetic intervention in mice. *Nat. Protoc.* **8**, 1475–1493 (2013).
3. E. Krook-Magnuson, C. Armstrong, M. Oijala, I. Soltesz, On-demand optogenetic control of spontaneous seizures in temporal lobe epilepsy. *Nat. Commun.* **4**, 1376 (2013).
4. A. D. Bui, T. M. Nguyen, C. Limouse, H. K. Kim, G. G. Szabo, S. Felong, M. Maroso, I. Soltesz, Dentate gyrus mossy cells control spontaneous convulsive seizures and spatial memory. *Science* **359**, 787–790 (2018).
5. S. Dong, S. C. Rogan, B. L. Roth, Directed molecular evolution of DREADDs: A generic approach to creating next-generation RASSLs. *Nat. Protoc.* **5**, 561–573 (2010).
6. D. M. Kullmann, S. Schorge, M. C. Walker, R. C. Wykes, Gene therapy in epilepsy—Is it time for clinical trials? *Nat. Rev. Neurol.* **10**, 300–304 (2014).
7. M. A. Vogelbaum, M. K. Aghi, Convection-enhanced delivery for the treatment of glioblastoma. *Neuro-Oncol.* **17**, ii3–ii8 (2015).
8. O. Lewis, M. Woolley, D. Johnson, A. Rosser, N. U. Barua, A. S. Bienemann, S. S. Gill, S. Evans, Chronic, intermittent convection-enhanced delivery devices. *J. Neurosci. Methods* **259**, 47–56 (2016).
9. R. Raghavan, M. L. Brady, M. I. Rodríguez-Ponce, A. Hartlep, C. Pedain, J. H. Sampson, Convection-enhanced delivery of therapeutics for brain disease, and its optimization. *Neurosurg. Focus* **20**, E12 (2006).
10. P. Kwan, S. C. Schachter, M. J. Brodie, Drug-resistant epilepsy. *N. Engl. J. Med.* **365**, 919–926 (2011).
11. W. Löscher, H. Klitgaard, R. E. Twyman, D. Schmidt, New avenues for anti-epileptic drug discovery and development. *Nat. Rev. Drug Discov.* **12**, 757–776 (2013).
12. M. Bialer, H. S. White, Key factors in the discovery and development of new antiepileptic drugs. *Nat. Rev. Drug Discov.* **9**, 68–82 (2010).
13. D. T. Simon, S. Kurup, K. C. Larsson, R. Hori, K. Tybrandt, M. Goiny, E. W. H. Jager, M. Berggren, B. Canlon, A. Richter-Dahlfors, Organic electronics for precise delivery of neurotransmitters to modulate mammalian sensory function. *Nat. Mater.* **8**, 742–746 (2009).
14. J. Isaksson, P. Kjäll, D. Nilsson, N. Robinson, M. Berggren, A. Richter-Dahlfors, Electronic control of $Ca^{2+}$ signalling in neuronal cells using an organic electronic ion pump. *Nat. Mater.* **6**, 673–679 (2007).
15. A. Jonsson, Z. Song, D. Nilsson, B. A. Meyerson, D. T. Simon, B. Linderoth, M. Berggren, Therapy using implanted organic bioelectronics. *Sci. Adv.* **1**, e1500039 (2015).
16. A. Williamson, J. Rivnay, L. Kergoat, A. Jonsson, S. Inal, I. Uguz, M. Ferro, A. Ivanov, T. Arbring Sjöström, D. T. Simon, M. Berggren, G. G. Malliaras, C. Bernard, Controlling epileptiform activity with organic electronic ion pumps. *Adv. Mater.* **27**, 3138–3144 (2015).
17. D. J. Poxson, M. Karady, R. Gabrielsson, A. Y. Alkattan, A. Gustavsson, S. M. Doyle, S. Robert, K. Ljung, M. Grebe, D. T. Simon, M. Berggren, Regulating plant physiology with organic electronics. *Proc. Natl. Acad. Sci. U.S.A.* **114**, 4597–4602 (2017).
18. A. Jonsson, S. Inal, I. Uguz, A. J. Williamson, L. Kergoat, J. Rivnay, D. Khodagholy, M. Berggren, C. Bernard, G. G. Malliaras, D. T. Simon, Bioelectronic neural pixel: Chemical stimulation and electrical sensing at the same site. *Proc. Natl. Acad. Sci. U.S.A.* **113**, 9440–9445 (2016).
19. A. Jonsson, T. A. Sjöström, K. Tybrandt, M. Berggren, D. T. Simon, Chemical delivery array with millisecond neurotransmitter release. *Sci. Adv.* **2**, e1601340 (2016).
20. I. Uguz, C. M. Proctor, V. F. Curto, A.-M. Pappa, M. J. Donahue, M. Ferro, R. M. Owens, D. Khodagholy, S. Inal, G. G. Malliaras, A microfluidic ion pump for in vivo drug delivery. *Adv. Mater.* **29**, 1701217 (2017).
21. J. Charmet, O. Banakh, E. Laux, B. Graf, F. Dias, A. Dunand, H. Keppner, G. Gorodyska, M. Textor, W. Noell, N. F. de Rooij, A. Neels, M. Dadras, A. Dommann, H. Knapp, C. Borter, M. Benkhaira, Solid on liquid deposition. *Thin Solid Films* **518**, 5061–5065 (2010).
22. J. Rivnay, R. M. Owens, G. G. Malliaras, The rise of organic bioelectronics. *Chem. Mater.* **26**, 679–685 (2014).
23. E. Syková, C. Nicholson, Diffusion in brain extracellular space. *Physiol. Rev.* **88**, 1277–1340 (2008).
24. M. E. Rice, G. A. Gerhardt, P. M. Hierl, G. Nagy, R. N. Adams, Diffusion coefficients of neurotransmitters and their metabolites in brain extracellular fluid space. *Neuroscience* **15**, 891–902 (1985).
25. P. A. Rutecki, F. J. Lebeda, D. Johnston, Epileptiform activity induced by changes in extracellular potassium in hippocampus. *J. Neurophysiol.* **54**, 1363–1374 (1985).
26. J. L. Stringer, E. W. Lothman, Epileptiform discharges induced by altering extracellular potassium and calcium in the rat hippocampal slice. *Exp. Neurol.* **101**, 147–157 (1988).
27. M. Szente, A. Baranyi, Mechanism of aminopyridine-induced ictal seizure activity in the cat neocortex. *Brain Res.* **413**, 368–373 (1987).
28. A. Baranyi, O. Fehér, Convulsive effects of 3-aminopyridine on cortical neurones. *Electroencephalogr. Clin. Neurophysiol.* **47**, 745–751 (1979).
29. H. Pasantes-Morales, M. E. Arzate, Effect of taurine on seizures induced by 4-aminopyridine. *J. Neurosci. Res.* **6**, 465–474 (1981).
30. M. Szente, F. Pongrácz, Comparative study of aminopyridine-induced seizure activities in primary and mirror foci of cat's cortex. *Electroencephalogr. Clin. Neurophysiol.* **52**, 353–367 (1981).
31. J. Mitterdorfer, B. P. Bean, Potassium currents during the action potential of hippocampal CA3 neurons. *J. Neurosci.* **22**, 10106–10115 (2002).
32. I. Osorio, M. G. Frei, J. Giftakis, T. Peters, J. Ingram, M. Turnbull, M. Herzog, M. T. Rise, S. Schaffner, R. A. Wennberg, T. S. Walczak, M. W. Risinger, C. Ajmone-Marsan, Performance reassessment of a real-time seizure-detection algorithm on long ECoG series. *Epilepsia* **43**, 1522–1535 (2002).
33. C. Szabó, L. C. Morgan, K. M. Karkar, L. D. Leary, O. V. Lie, M. Girouard, J. E. Cavazos, Electromyography-based seizure detector: Preliminary results comparing a generalized tonic–clonic seizure detection algorithm to video-EEG recordings. *Epilepsia* **56**, 1432–1437 (2015).
34. S. Ramgopal, S. Thome-Souza, M. Jackson, N. E. Kadish, I. Sánchez Fernández, J. Klehm, W. Bosl, C. Reinsberger, S. Schachter, T. Loddenkemper, Seizure detection, seizure prediction, and closed-loop warning systems in epilepsy. *Epilepsy Behav.* **37**, 291–307 (2014).
35. W. C. Stacey, Seizure prediction is possible–now let's make it practical. *EBioMedicine* **27**, 3–4 (2018).
36. C. Nicholson, Interaction between diffusion and Michaelis-Menten uptake of dopamine after iontophoresis in striatum. *Biophys. J.* **68**, 1699–1715 (1995).
37. J. S. Isaacson, J. M. Solís, R. A. Nicoll, Local and diffuse synaptic actions of GABA in the hippocampus. *Neuron* **10**, 165–175 (1993).
38. S. Ramakrishna, J. Mayer, E. Wintermantel, K. W. Leong, Biomedical applications of polymer-composite materials: A review. *Compos. Sci. Technol.* **61**, 1189–1224 (2001).
39. J. P. Santerre, K. Woodhouse, G. Laroche, R. S. Labow, Understanding the biodegradation of polyurethanes: From classical implants to tissue engineering materials. *Biomaterials* **26**, 7457–7470 (2005).
40. J. M. Morais, F. Papadimitrakopoulos, D. J. Burgess, Biomaterials/tissue interactions: Possible solutions to overcome foreign body response. *AAPS J.* **12**, 188–196 (2010).
41. A. Lecomte, E. Descamps, C. Bergaud, A review on mechanical considerations for chronically-implanted neural probes. *J. Neural Eng.* **15**, 031001 (2018).
42. F. T. Sun, M. J. Morrell, R. E. Wharen, Responsive cortical stimulation for the treatment of epilepsy. *Neurotherapeutics* **5**, 68–74 (2008).
43. B. Rosin, M. Slovik, R. Mitelman, M. Rivlin-Etzion, S. N. Haber, Z. Israel, E. Vaadia, H. Bergman, Closed-loop deep brain stimulation is superior in ameliorating parkinsonism. *Neuron* **72**, 370–384 (2011).

44. J. Herron, T. Denison, H. J. Chizeck, in *2015 7th International IEEE/EMBS Conference on Neural Engineering* (NER), Montpellier, France, 22 to 24 April 2015.
45. M.-C. Picot, M. Baldy-Moulinier, J.-P. Daurès, P. Dujols, A. Crespel, The prevalence of epilepsy and pharmacoresistant epilepsy in adults: A population-based study in a Western European country. *Epilepsia* **49**, 1230–1238 (2008).
46. S. Pati, A. V. Alexopoulos, Pharmacoresistant epilepsy: From pathogenesis to current and emerging therapies. *Cleve. Clin. J. Med.* **77**, 457–467 (2010).
47. A. Hufnagel, M. Dümpelmann, J. Zentner, O. Schijns, C. E. Elger, Clinical relevance of quantified intracranial interictal spike activity in presurgical evaluation of epilepsy. *Epilepsia* **41**, 467–478 (2000).

**Acknowledgments:** We thank I. Uguz, S. Inal, V. Curto, M. Donahue, M. Ferro, and Z. Maglóczky for fruitful discussions. **Funding:** A.K. was sponsored by the Marie Curie Intra-European Fellowship for Career Development (no. 625372). C.M.P. acknowledges funding from a Whitaker International Scholar grant administered by the Institute for International Education. A.W. acknowledges funding from the European Research Council under the European Union's Horizon 2020 Research and Innovation Programme (grant agreement no. 716867) and from the Excellence Initiative of Aix-Marseille University (A*MIDEX), a French "Investissements d'Avenir" programme. C.B. acknowledges funding from the A*MIDEX project MIDOE (A_M-AAP-ID-13-24-130531-16.31-BERNARD-HLS). **Author contributions:** G.G.M., A.W., C.M.P., and C.B. conceived the project. C.M.P. designed and fabricated the μFIP devices. A.W., C.M.P., A.S., A.G., and C.B. designed and executed in vivo experiments. A.S. and A.G. performed animal surgeries. A.S. and A.K. performed histology analysis. A.S. and A.W. analyzed electrophysiology recordings. I.d.A. and A.-M.P. performed ELISA kit analysis. C.M.P. drafted the manuscript with input from all authors. **Competing interests:** The authors declare that they have no competing interests. **Data and materials availability:** All data needed to evaluate the conclusions in the paper are present in the paper and/or the Supplementary Materials. Additional data related to this paper may be requested from the authors.

Submitted 9 May 2018
Accepted 19 July 2018
Published 29 August 2018
10.1126/sciadv.aau1291

**Citation:** C. M. Proctor, A. Slézia, A. Kaszas, A. Ghestem, I. del Agua, A.-M. Pappa, C. Bernard, A. Williamson, G. G. Malliaras, Electrophoretic drug delivery for seizure control. *Sci. Adv.* **4**, eaau1291 (2018).